



CERN-EP-2022-055
17 March 2022

**System-size dependence of the charged-particle pseudorapidity density at
 $\sqrt{s_{\text{NN}}} = 5.02$ TeV for pp, p–Pb, and Pb–Pb collisions**

ALICE Collaboration

Abstract

We present and compare the charged-particle pseudorapidity densities for pp, p–Pb, and Pb–Pb collisions at $\sqrt{s_{\text{NN}}} = 5.02$ TeV measured over a wide pseudorapidity range ($-3.5 < \eta < 5$), using ALICE at the Large Hadron Collider. The distributions for p–Pb and Pb–Pb collisions are determined as a function of the centrality of the collisions, while results from pp collisions are reported for inelastic events with at least one charged particle at midrapidity. The charged-particle pseudorapidity densities are, under simple and robust assumptions, transformed to charged-particle rapidity densities. This allows for the calculation and the presentation of the evolution of the width of the rapidity distributions and of a lower bound on the Bjorken energy density, as a function of the number of participants in all three collision systems. We find a decreasing width of the particle production, and roughly a ten fold increase in the energy density, as the system size grows.

arXiv:2204.10210v1 [nucl-ex] 21 Apr 2022

1 Introduction

The number of charged particles produced in energetic nuclear collisions is an important indicator for the strong interaction processes that determine the particle production at the sub-nucleonic level. In particular, the production of charged particles is expected to reflect the number of quark and gluon collisions occurring during the initial stages of the reaction. The total number of particles produced also provides information on the energy transfer available from the initial colliding beams to particle production, as a consequence of nuclear stopping [1]. In order to help unravel this complex scenario it is important to compare the particle production amongst collision systems of different sizes over a wide kinematic range.

We present the measured charged-particle pseudorapidity density, $dN_{\text{ch}}/d\eta$, for pp, p–Pb, and Pb–Pb collisions at the same collision energy of $\sqrt{s_{\text{NN}}} = 5.02 \text{ TeV}$ in the nucleon–nucleon centre-of-mass reference frame. This is, at present, the maximum available energy at CERN’s Large Hadron Collider (LHC) for Pb–Pb collisions. The measurements were carried out using ALICE at LHC. The three studied reactions have different characteristics probing widely different particle production yields and mechanisms. In Pb–Pb collisions, the total particle yield for central collisions is of the order 10^4 [2] and a strongly coupled plasma of quarks and gluons (sQGP) is formed [3, 4, 5, 6], whose collective and transport properties are currently under intense study. On the other hand, pp collisions represent the simplest possible nuclear collision system, where the average total particle production is much smaller (≈ 80), and is to first approximation much less subject to collective effects. The p–Pb system is intermediate to the other reactions corresponding to the situation where a single nucleon probes the nucleons in a narrow cylinder of the target nucleus. The extent to which p–Pb is governed by the initial state cold nuclear matter of the lead ion or whether collective phenomena in the hot and dense medium play an important role is, at present, a matter under scrutiny by the community.

In this letter, we compare the three reactions and present the ratios of the charged-particle pseudorapidity density distributions ($dN_{\text{ch}}/d\eta$) of the more complex reactions to the pp distribution. Using simple and robust assumptions, we transform the measured charged-particle pseudorapidity density distributions into charged-particle rapidity density distributions (dN_{ch}/dy). This allows us to calculate the width of the rapidity distributions as a function of the number of participating nucleons. The parameters of the transformation also allow us to estimate a lower bound on the energy density using the well-known formula from Bjorken [7]. An energy density exceeding the critical energy density of roughly $1 \text{ GeV}/\text{fm}^3$ [8] is a necessary condition for the formation of deconfined matter of quarks and gluons, and thus it is of the utmost interest to understand the development of these energy densities across different collision systems.

2 Experimental setup, data sample, analysis method, systematic uncertainties

A detailed description of the ALICE detector and its performance can be found elsewhere [9, 10]. The present analysis uses the Silicon Pixel Detector (SPD) to determine the pseudorapidity densities in the range $-2 < \eta < 2$ and the Forward Multiplicity Detector (FMD) in the ranges $-3.5 < \eta < -1.8$ and $1.8 < \eta < 5$. The V0, comprised of two plastic scintillator discs covering $-3.7 < \eta < -1.7$ (V0C) and $2.8 < \eta < 5.1$ (V0A), and the ZDC, two zero-degree calorimeters located 112.5 m from the interaction point, measurements determine the collision centrality and provide the offline event trigger [2].

The results presented are based on data from collisions at a centre-of-mass energy per nucleon pair of $\sqrt{s_{\text{NN}}} = 5.02 \text{ TeV}$ as collected by ALICE during LHC Run 1 (2013) for p–Pb, and during Run 2 (2015) for pp and Pb–Pb. About 10^5 events with a minimum bias trigger requirement [11] were analysed in the centrality range from 0% to 90% and 0% to 100% of the visible cross section for Pb–Pb and p–Pb collisions, respectively. The minimum bias trigger for p–Pb and Pb–Pb collisions in ALICE was defined as a coincidence between the V0A and V0C sides of the V0 detector.

The data from the p–Pb collisions were taken in two beam configurations: one where the lead ion travelled toward positive pseudorapidity and one where it travelled toward negative pseudorapidity. The results from the latter collisions are mirrored around $\eta = 0$. The centre-of-mass frame in p–Pb collisions does not coincide with the laboratory frame, due to the single magnetic field in the LHC, and thus the rapidity of the centre-of-mass is $y_{\text{CM}} = \pm 0.465$ for the two directions, respectively, in the laboratory frame. For this reason, pseudorapidity, calculated with respect to the laboratory frame, is denoted η_{lab} whenever p–Pb results are presented.

Likewise, for the pp collisions, about 10^5 events with coincidence between V0A and V0C and at least one charged particle in $|\eta| < 1$ were analysed. By requiring at least one charged particle at midrapidity, the so-called INEL>0 event class, the systematic uncertainty, related to the absolute normalisation to the full inelastic cross section, is reduced, while still sampling a large fraction of the hadronic cross section [12, 13].

The standard ALICE event selection [14] and centrality estimator based on the V0 amplitude [15, 16] are used in this analysis. The event selection consists of: a) exclusion of background events using the timing information from the ZDC (for Pb–Pb and p–Pb, e.g., beam–gas interactions) and V0 detectors, b) verification of the trigger conditions, and c) a reconstructed position of the collision. In Pb–Pb collisions, centrality is obtained from the sum amplitude in both V0 detector arrays (V0M). For p–Pb only the amplitude in the array on the lead-going side (V0A or V0C) is used. In Pb–Pb collisions, the 10% most peripheral collisions have substantial contributions from electromagnetic processes and are therefore not included in the results presented here [15].

A primary charged particle is defined as a charged particle with a mean proper lifetime τ larger than $1 \text{ cm}/c$, which is either a) produced directly in the interaction, or b) from decays of particles with τ smaller than $1 \text{ fm}/c$ [17]. All quantities reported are for primary, charged particles, though “primary” is omitted in the following for brevity.

The analysis method is identical to that of previous publications [2]: the measurement of the charged-particle pseudorapidity density at midrapidity is obtained from counting particle trajectories determined using the two layers of the SPD. In the forward regions, the measurement is provided by the analysis of the deposited energy signal in the FMD and a statistical method is employed to calculate the inclusive number of charged particles. A data-driven correction [18], based on separate measurements exploiting displaced collision vertices, is applied to remove the background from secondary particles.

Systematic uncertainty estimations for the midrapidity measurements are detailed elsewhere [2, 12, 16], and are obtained through variation of thresholds, simulation studies, and so on. For pp (p–Pb), the total systematic uncertainty amounts to 1.5% (2.7%) over the whole pseudorapidity range; while for Pb–Pb the total systematic uncertainty is 2.6% at $\eta = 0$ and 2.9% at $|\eta| = 2$. The systematic uncertainty is mostly correlated over $|\eta| < 2$, and largely independent of centrality. The uncertainty in the forward region, estimated via variations of thresholds and simulation studies, is the same for all collision systems and is uncorrelated across η , amounting to 6.9% for $\eta > 3.5$ and 6.4% elsewhere within the forward regions [18]. In the figures of this letter, uncorrelated systematic uncertainties are indicated by open boxes on the data points, while correlated systematic uncertainties, those that affect the overall scale, are indicated by filled boxes to the right of the data. The systematic uncertainty on $dN_{\text{ch}}/d\eta$, due to the centrality class definition in Pb–Pb, is estimated to vary from 0.6% for the most central to 9.5% for the most peripheral class [19]. The 80% to 90% centrality class has residual contamination from electromagnetic processes as detailed elsewhere [15], which gives rise to an additional 4% systematic uncertainty in the measurements.

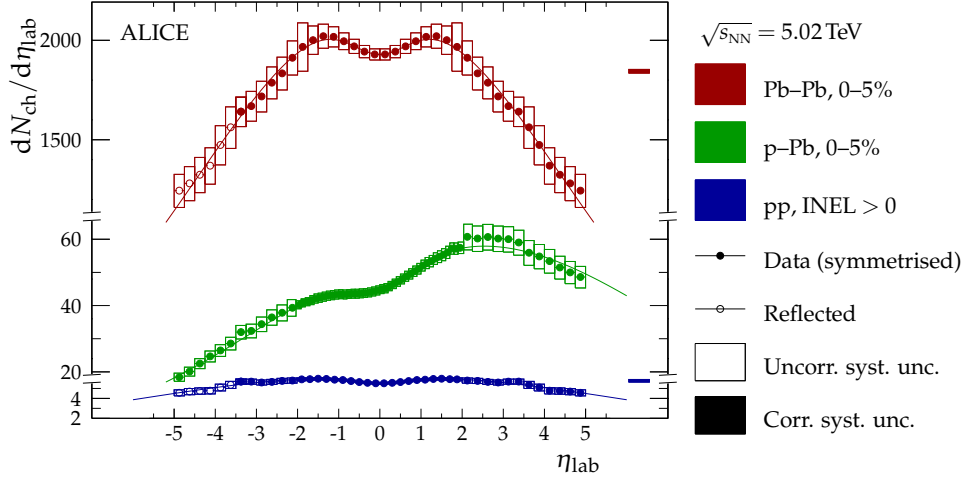


Figure 1: Charged-particle pseudorapidity density in Pb–Pb [2] and p–Pb for the 5% most central collisions, and for pp collisions with INEL>0 trigger class. For symmetric collision systems (Pb–Pb and pp) the data has been symmetrised around $\eta = 0$ and points for $\eta > 3.5$ have been reflected around $\eta = 0$. The lines show fits of Eq. (1) (Pb–Pb and pp) and Eq. (2) (p–Pb) to the data (see text). Please note that the ordinate has been cut twice to accommodate for the very different ranges of the charged-particle pseudorapidity densities.

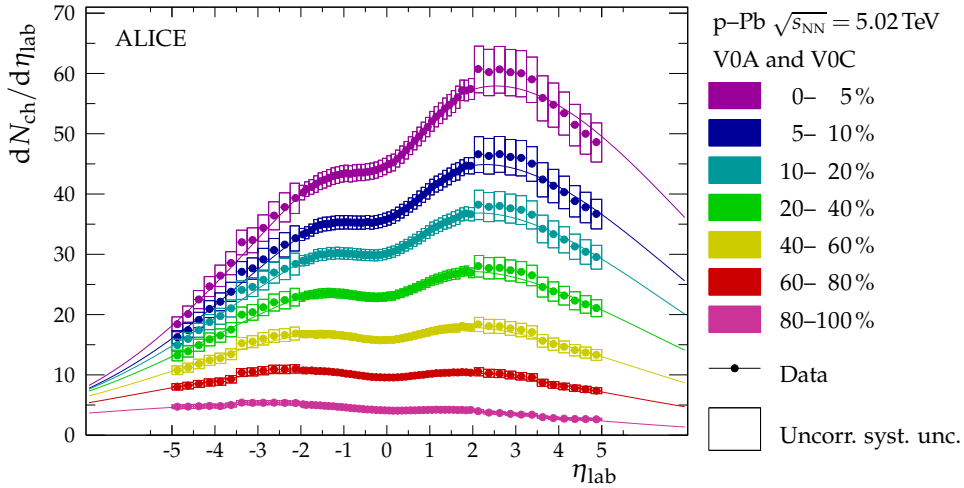


Figure 2: Charged-particle pseudorapidity density in p–Pb collisions at $\sqrt{s_{\text{NN}}} = 5.02$ TeV in seven centrality classes based on the V0A and V0C estimators. The lines are obtained using a fit of a scaled, normal distribution in rapidity Eq. (2) to the data (see text for details).

3 Results

Figure 1 shows the measured pseudorapidity densities in pp, and in central p–Pb, and the previously published results for Pb–Pb [2] collisions at $\sqrt{s_{\text{NN}}} = 5.02$ TeV for primary particles.

For the 5% most central Pb–Pb collisions $dN_{\text{ch}}/d\eta \approx 2000$ at midrapidity [2], while for p–Pb collisions the distribution peaks at $dN_{\text{ch}}/d\eta_{\text{lab}} \approx 60$ around $\eta = 3$ on the lead-going direction ($\eta > 0$). For pp collisions with the INEL>0 trigger condition discussed above, $dN_{\text{ch}}/d\eta = 5.7 \pm 0.2$ at midrapidity, consistent with previous results derived from p_{T} spectra [20].

Figure 2 shows, as a function of centrality, the measured charged-particle pseudorapidity densities for p–Pb collisions at $\sqrt{s_{\text{NN}}} = 5.02$ TeV. The strategy of centrality selection for proton on nucleus reactions is explained elsewhere [16]. The ALICE Collaboration has previously presented similar distributions

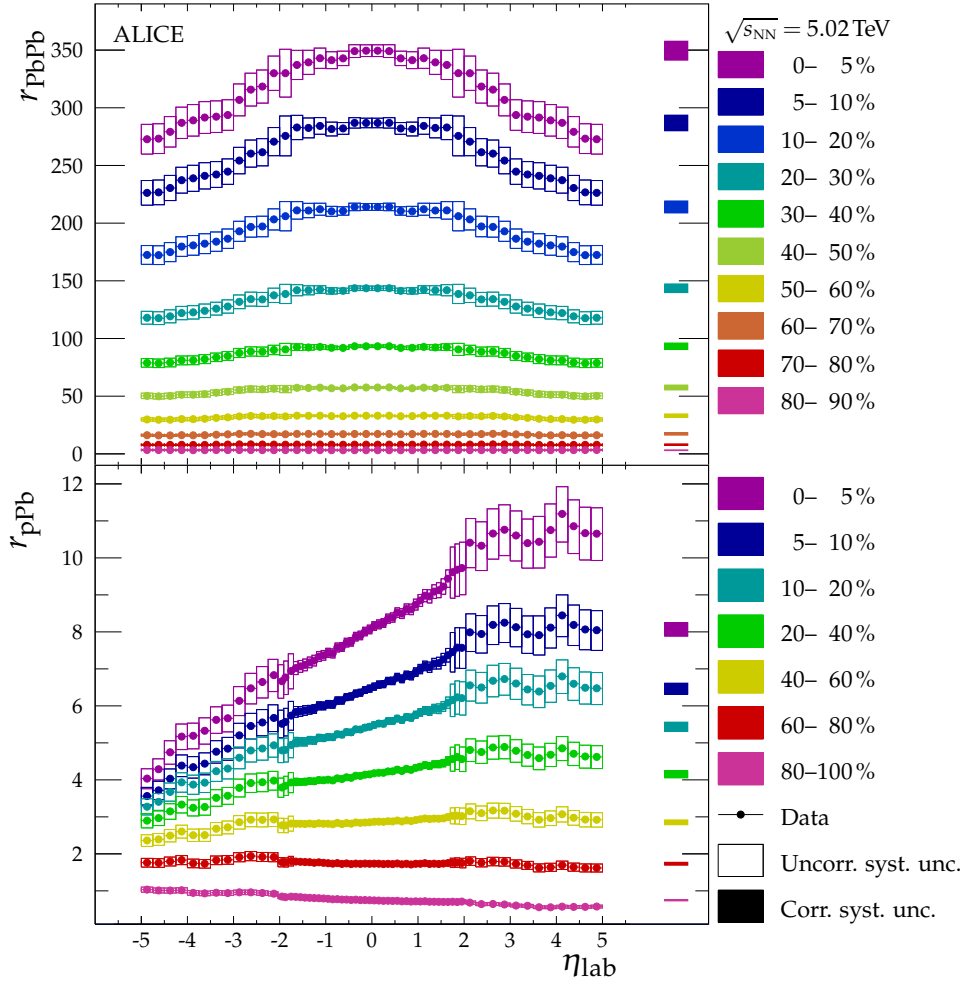


Figure 3: Ratio r_X of the charged-particle pseudorapidity density in Pb-Pb (top) and p-Pb (bottom) in different centrality classes to the charged-particle pseudorapidity density in pp in the INEL>0 event class. Note, for Pb-Pb η_{lab} is the same as the centre-of-mass pseudorapidity.

and curves for Pb-Pb collisions at this energy [2].

In Fig. 3, the charged-particle pseudorapidity densities in p-Pb and Pb-Pb reactions are divided by the pp distributions corresponding to the INEL>0 trigger class. The ratio is $r_X = (dN_{\text{ch}}/d\eta|_X)/(dN_{\text{ch}}/d\eta|_{\text{pp}})$, where X labels centrality classes in p-Pb and Pb-Pb. In the ratios, systematic uncertainties are partially cancelled, and the magnitude of the resulting systematic uncertainties are given by the uncertainties in the $dN_{\text{ch}}/d\eta|_X$ measurements. In p-Pb collisions the rapidity of the centre-of-mass is non-zero which is not taken into account in the ratios. Such a correction would require prior determination of the full Jacobian of the transformation from pseudorapidity to rapidity, which is not possible with the ALICE apparatus.

The ratio of the p-Pb relative to the pp distributions increases with pseudorapidity from the p-going to the Pb-going direction for central collisions, suggesting a scaling of the pp distribution with the increasing number of participants as the lead nucleus is probed by the incident proton, indicative of independent proton-nucleon scatterings on the lead-ion side [21, 22]. A similar scaling, however, does not hold for the Pb-Pb reaction. The ratios cannot be obtained by simple scaling of the elementary pp distributions. Instead, the ratio of the Pb-Pb relative to the pp distributions exhibits an enhancement of particle production around midrapidity for the more central collisions that is indicative of the formation of the sQGP [4]. Likewise, r_{pPb} increases for all but the two most peripheral centrality classes as $\eta \rightarrow 3$, suggesting that

the various mechanisms behind the pseudorapidity distributions are more transversely directed in peripheral p–Pb than in pp collisions (the same observation also holds for Pb–Pb with respect to pp collisions).

4 Rapidity and energy-density dependence on system size and discussion

It has been shown that the charged-particle *rapidity* density (dN_{ch}/dy) in Pb–Pb collisions, to a good accuracy, follows a normal distribution over the considered rapidity interval ($|y| \lesssim 5$) [2, 23]. Those results relied on calculating the average Jacobian $d\eta/dy = \langle J \rangle = \langle \beta \rangle$ using the full p_{T} spectra, at midrapidity, of charged pions and kaons as well as protons and antiprotons. Here, we use the approximation

$$y \approx \eta - \frac{1}{2} \frac{m^2}{p_{\text{T}}^2} \cos \vartheta,$$

where ϑ is the polar angle of emission, and identify $a = p_{\text{T}}/m$ with an effective ratio of transverse momentum over mass. With this, the effective Jacobian can be written as

$$J'(\eta, a) = \left(1 + \frac{1}{a^2} \frac{1}{\cosh^2 \eta} \right)^{-1/2}.$$

We further make the ansatz that dN_{ch}/dy is normal distributed for symmetric collision systems (pp and Pb–Pb), so that $dN_{\text{ch}}/d\eta$ can be parameterised as

$$f(\eta; A, a, \sigma) = J'(\eta, a) A \frac{1}{\sqrt{2\pi}\sigma} \exp\left(-\frac{y^2\{\eta, a\}}{2\sigma^2}\right), \quad (1)$$

where A and σ are the total integral and width of the distribution, respectively, and y the rapidity in the centre-of-mass frame. Motivated by the observed approximate linearity of r_{pPb} (see lower panel of Fig. 3), we replace A with $(\alpha y + A)$ for the asymmetric system (p–Pb) and parameterise $dN_{\text{ch}}/d\eta_{\text{lab}}$ as

$$g(\eta; A, a, \alpha, \sigma) = J'(\eta, a) (\alpha y\{\eta, a\} + A) \frac{1}{\sqrt{2\pi}\sigma} \exp\left(-\frac{[y(\{\eta, a\}) - y_{\text{CM}}]^2}{2\sigma^2}\right). \quad (2)$$

The functions f and g defined in Eq. (1) and Eq. (2), respectively, describe the measurements within the measured region with χ^2 per degrees of freedom (ν) in the range of 0.1 to 0.5. That is, the charged-particle distributions for pp, p–Pb, and Pb–Pb collisions at $\sqrt{s_{\text{NN}}} = 5.02$ TeV follow a normal distribution in rapidity.

The top panel of Fig. 4 shows the best-fit parameter values of the normal width ($\sigma_{dN_{\text{ch}}/dy}$) for all three collision systems as a function of the average number of participating nucleons ($\langle N_{\text{part}} \rangle$) calculated using a Glauber model [24]. The result using the above procedure, for the most central Pb–Pb collisions, is found to be compatible with previous results extracted by unfolding with the mean Jacobian estimated from transverse momentum spectra [2]. The open points (crosses) and dashed lines on the figure are from evaluations of Eq. (1) and Eq. (2), and direct calculations of $\sigma_{dN_{\text{ch}}/dy}$, respectively, using model calculations with EPOS-LHC [25]. EPOS-LHC was chosen as it provides predictions for all three collision systems. The parameterisation, in terms of the two functions, of this model calculation generally reproduces the widths of the charged-particle rapidity densities, except in the asymmetric case where a direct evaluation of the standard deviation is less motivated.

The general trend is that the widths decrease as $\langle N_{\text{part}} \rangle$ increases, consistent with the behaviour of the r_{pPb} ratios. Notably, the width of the dN_{ch}/dy distributions in p–Pb and Pb–Pb, for low number of participant nucleons in the collisions, approaches the width of the pp distribution, which, presumably, is dominated by kinematic and phase space constraints.

The lower panel of Fig. 4 shows the dependence of a on the average number of participants. The right-hand ordinate is the same, but multiplied by the average mass $\langle m \rangle = (0.215 \pm 0.001)$ GeV/ c^2 estimated

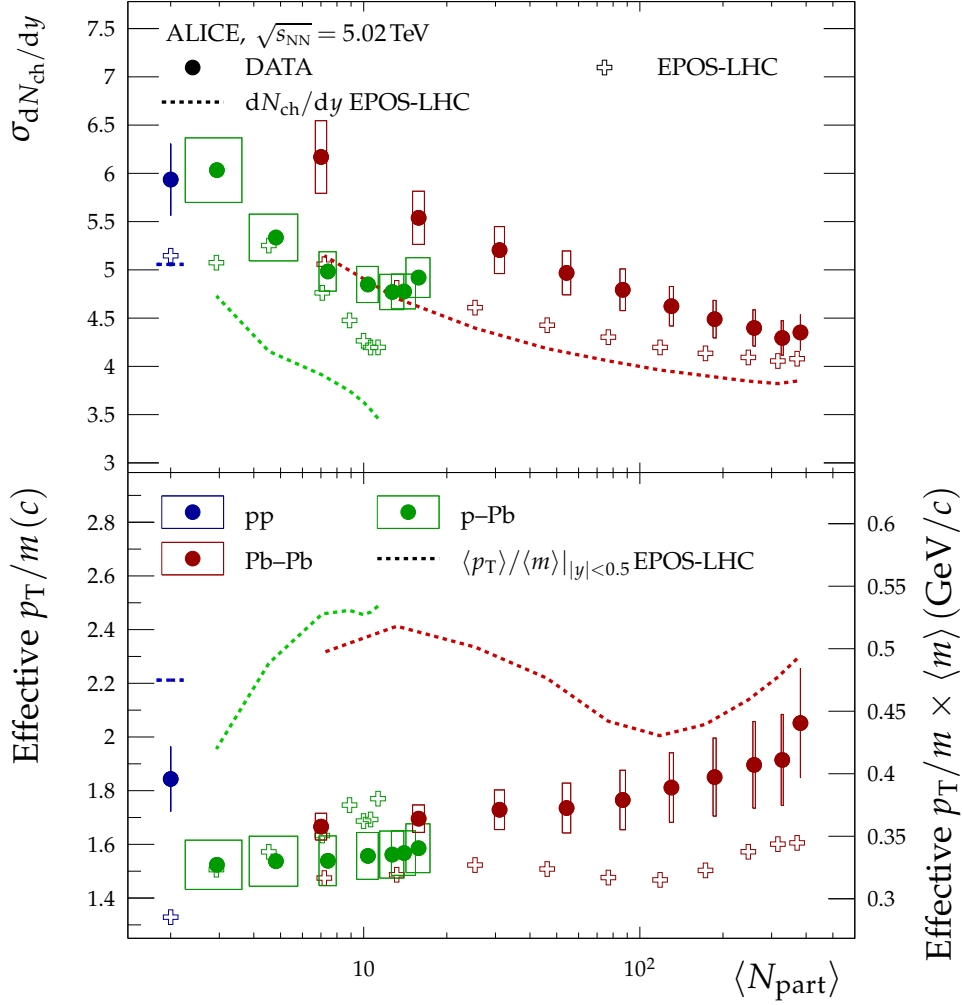


Figure 4: The width (top) and effective p_{T}/m (bottom) fit parameters as a function of the mean number of participants in pp, p–Pb, and Pb–Pb collisions at $\sqrt{s_{\text{NN}}} = 5.02$ TeV. Vertical uncertainties are the standard error on the best-fit parameter values, while horizontal uncertainties reflect the uncertainty on $\langle N_{\text{part}} \rangle$ from the Glauber calculations. Also shown are similar fit parameters from the same parameterisation of EPOS-LHC calculations as well as the relevant numbers extracted directly from those calculations.

from measurements of identified particles [26]. To better understand the parameter a , this parameter extracted from the EPOS-LHC calculations using the above procedure is also shown in the figure. The dotted lines show the average p_{T}/m predicted by EPOS-LHC [25]. The EPOS-LHC calculations indicate that the extracted effective transverse momentum to mass ratio a is smaller than the ratio of the average transverse momentum to the average mass.

We can estimate the energy density that is reached in the collisions as a function of the number of participants for the three systems. A conventional approach is to use the model originally proposed by Bjorken [7] in which the energy density (ϵ_{Bj}) depends on the rapidity density of particles and the volume of a longitudinal cylinder with cross sectional area determined by the overlap between the colliding partners and length determined by a characteristic particle formation time

$$\epsilon_{\text{Bj}} = \frac{1}{c\tau} \frac{1}{S_{\text{T}}} \left\langle \frac{dE_{\text{T}}}{dy} \right\rangle.$$

Here, $S_{\text{T}} \approx \pi R^2 \approx \pi N_{\text{part}}^{2/3}$ is the transverse area spanned by the participating nucleons, dE_{T}/dy is the transverse-energy rapidity density, and τ is the formation time. While a formation time of $\tau = 1$ fm/c

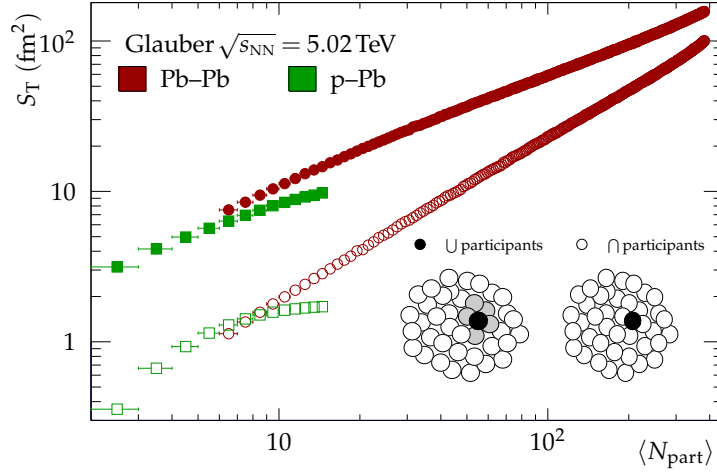


Figure 5: The transverse area S_T as calculated in a numerical Glauber model for two extreme cases: a) only the exclusive overlap of nucleons is considered (\cap , open markers) and b) the inclusive area of participating nucleons contribute (\cup , closed markers) in both p-Pb and Pb-Pb at $\sqrt{s_{\text{NN}}} = 5.02$ TeV.

is often assumed, it is left as a free parameter here. With $\langle m_T \rangle = \langle m \rangle \sqrt{1 + (\langle p_T \rangle / \langle m \rangle)^2}$, the transverse-energy rapidity density can be approximated by

$$\left\langle \frac{dE_T}{dy} \right\rangle \approx \langle m_T \rangle \frac{1}{f_{\text{total}}} \frac{dN_{\text{ch}}}{dy} = \langle m \rangle \sqrt{1 + \left(\frac{\langle p_T \rangle}{\langle m \rangle} \right)^2} \frac{1}{f_{\text{total}}} \frac{dN_{\text{ch}}}{dy},$$

where $f_{\text{total}} = 0.55 \pm 0.01$, the ratio of charged particles to all particles [27], accounts for neutral particles not measured in the experiment, and is assumed the same for all collision systems. Substituting the derived dN_{ch}/dy and the effective $a = p_T/m \lesssim \langle p_T \rangle / \langle m \rangle$ results in a lower bound estimate for the Bjorken energy density (ε_{LB})

$$\varepsilon_{\text{Bj}} \tau \geq \varepsilon_{\text{LB}} \tau = \frac{1}{c} \frac{1}{S_T} \langle m \rangle \sqrt{1 + a^2} \frac{1}{f_{\text{total}}} \sqrt{1 + \frac{1}{a^2} \frac{1}{\cosh^2 \eta} \frac{dN_{\text{ch}}}{d\eta}}.$$

The transverse area S_T is estimated in a numerical Glauber model [28, 29] as shown in Fig. 5. We consider two extremes for the transverse area spanned by the participating nucleons: a) the *exclusive* (or direct) overlap between participating nucleons, \cap and open markers in Fig. 5, and b) the *inclusive* (or full) area of all participating nucleons, \cup and full markers in Fig. 5.

Figure 6 shows the lower-bound energy density estimate, $\varepsilon_{\text{LB}} \tau \leq \varepsilon_{\text{Bj}} \tau$, as a function of the number of participants, which reaches values between 10 and 20 GeV/(fm²c) in the most central Pb-Pb collisions. A rise from roughly 1 GeV/(fm²c) to over 10 GeV/(fm²c) is observed if the transverse area is assumed to be the inclusive area of participating nucleons. This trend is illustrated by a power-law (CN_{part}^p) fit to the data in the figure, with the parameter values $C = (0.8 \pm 0.3)$ GeV/(fm²c) and $p = 0.44 \pm 0.08$. On the other hand, if the transverse area is assumed to be the smaller exclusive overlap area, we observe a substantially larger lower bound on the energy density, but a less dramatic increase with increasing number of participating nucleons. Also shown in the figure are similar estimates of the Bjorken energy density $\varepsilon_{\text{Bj}} \tau$ for Pb-Pb reactions at $\sqrt{s_{\text{NN}}} = 2.76$ TeV [27]. The trend of the $\sqrt{s_{\text{NN}}} = 5.02$ TeV results are similar to these earlier results. Bearing in mind that for the largest LHC collision energy we show a lower bound estimate of the energy density in Fig. 6, we find a likely overall increase in the energy density from $\sqrt{s_{\text{NN}}} = 2.76$ TeV to 5.02 TeV.

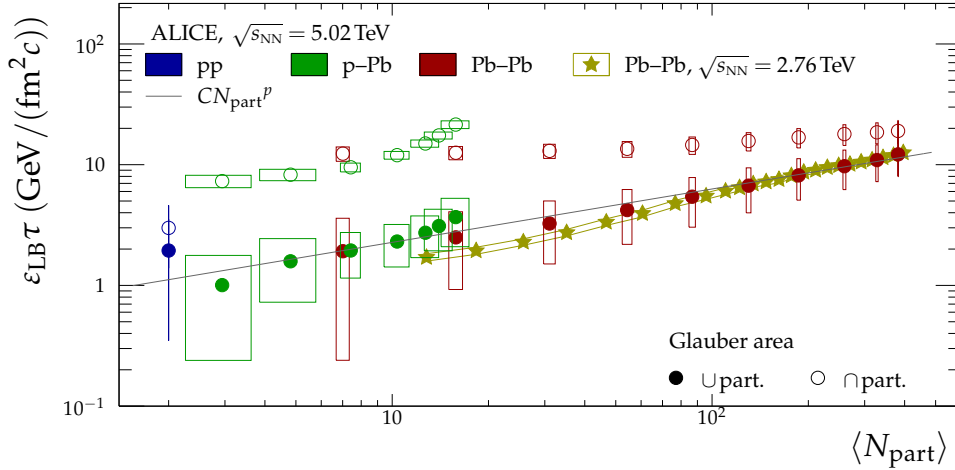


Figure 6: Estimate of the lower bound on the Bjorken transverse energy density in pp, p–Pb, and Pb–Pb collisions at $\sqrt{s_{\text{NN}}} = 5.02 \text{ TeV}$, considering the exclusive (\cap , open markers) and inclusive (\cup , full markers) overlap area S_T of the nucleons. The expression CN_{part}^p is fitted to case \cup , and we find $C = (0.8 \pm 0.3) \text{ GeV}/(\text{fm}^2c)$ and $p = 0.44 \pm 0.08$. Also shown is a similar estimate from Pb–Pb collisions at $\sqrt{s_{\text{NN}}} = 2.76 \text{ TeV}$ (stars with uncertainty band) [27].

5 Summary and conclusions

We have measured the charged particle pseudorapidity density in pp, p–Pb, and Pb–Pb collisions at $\sqrt{s_{\text{NN}}} = 5.02 \text{ TeV}$. While the particle production in central Pb–Pb collisions clearly exhibits an enhancement as compared to pp collisions, particle production in p–Pb collisions is consistent with dominantly incoherent nucleon–nucleon collisions. By transforming the measured pseudorapidity distributions to rapidity distributions we have obtained systematic trends for the width of the rapidity distributions and a lower bound on the energy density, which shows a clear scaling behaviour as a function of the average number of participant nucleons. The decreasing width of the deduced rapidity distributions with increasing participant number suggests that the kinematic spread of particles, including longitudinal degrees of freedom, is reduced due to interactions in the early stages of the collisions. This is also reflected in the accompanying growth of the energy density. Both observations are consistent with the gradual establishment of a high-density phase of matter with increasing size of the collision domain.

References

- [1] **BRAHMS** Collaboration, I. C. Arsene *et al.*, “Nuclear stopping and rapidity loss in Au+Au collisions at $\sqrt{s_{\text{NN}}} = 62.4 \text{ GeV}$ ”, *Phys. Lett. B* **677** (2009) 267–271, arXiv:0901.0872 [nucl-ex].
- [2] **ALICE** Collaboration, J. Adam *et al.*, “Centrality dependence of the pseudorapidity density distribution for charged particles in Pb–Pb collisions at $\sqrt{s_{\text{NN}}} = 5.02 \text{ TeV}$ ”, *Phys. Lett. B* **772** (2017) 567–577, arXiv:1612.08966 [nucl-ex].
- [3] **BRAHMS** Collaboration, I. Arsene *et al.*, “Quark gluon plasma and color glass condensate at RHIC? The Perspective from the BRAHMS experiment”, *Nucl. Phys. A* **757** (2005) 1–27, arXiv:nucl-ex/0410020 [nucl-ex].
- [4] **PHOBOS** Collaboration, B. B. Back *et al.*, “The PHOBOS perspective on discoveries at RHIC”, *Nucl. Phys. A* **757** (2005) 28–101, arXiv:nucl-ex/0410022 [nucl-ex].
- [5] **STAR** Collaboration, J. Adams *et al.*, “Experimental and theoretical challenges in the search for the quark gluon plasma: The STAR Collaboration’s critical assessment of the evidence from RHIC collisions”, *Nucl. Phys. A* **757** (2005) 102–183, arXiv:nucl-ex/0501009 [nucl-ex].

- [6] **PHENIX** Collaboration, K. Adcox *et al.*, “Formation of dense partonic matter in relativistic nucleus-nucleus collisions at RHIC: Experimental evaluation by the PHENIX collaboration”, *Nucl. Phys. A* **757** (2005) 184–283, arXiv:nucl-ex/0410003 [nucl-ex].
- [7] J. D. Bjorken, “Highly relativistic nucleus-nucleus collisions: The central rapidity region”, *Phys. Rev. D* **27** (Jan, 1983) 140–151.
- [8] H.-T. Ding, “Recent lattice QCD results and phase diagram of strongly interacting matter”, *Nucl. Phys. A* **931** (2014) 52–62, arXiv:1408.5236 [hep-lat].
- [9] **ALICE** Collaboration, K. Aamodt *et al.*, “The ALICE experiment at the CERN LHC”, *JINST* **3** (2008) S08002.
- [10] **ALICE** Collaboration, B. Abelev *et al.*, “Performance of the ALICE Experiment at the CERN LHC”, *Int. J. Mod. Phys. A* **29** (2014) 1430044, arXiv:1402.4476 [nucl-ex].
- [11] **ALICE** Collaboration, K. Aamodt *et al.*, “Centrality dependence of the charged-particle multiplicity density at mid-rapidity in Pb-Pb collisions at $\sqrt{s_{\text{NN}}} = 2.76 \text{ TeV}$ ”, *Phys. Rev. Lett.* **106** (2011) 032301, arXiv:1012.1657 [nucl-ex].
- [12] **ALICE** Collaboration, J. Adam *et al.*, “Charged-particle multiplicities in proton-proton collisions at $\sqrt{s} = 0.9$ to 8 TeV ”, *Eur. Phys. J. C* **77** no. 1, (2017) 33, arXiv:1509.07541 [nucl-ex].
- [13] **ALICE** Collaboration, S. Acharya *et al.*, “Pseudorapidity distributions of charged particles as a function of mid- and forward rapidity multiplicities in pp collisions at $\sqrt{s} = 5.02, 7$ and 13 TeV ”, *Eur. Phys. J. C* **81** no. 7, (2021) 630, arXiv:2009.09434 [nucl-ex].
- [14] **ALICE** Collaboration, K. Aamodt *et al.*, “Charged-particle multiplicity density at mid-rapidity in central Pb-Pb collisions at $\sqrt{s_{\text{NN}}} = 2.76 \text{ TeV}$ ”, *Phys. Rev. Lett.* **105** (2010) 252301, arXiv:1011.3916 [nucl-ex].
- [15] **ALICE** Collaboration, B. Abelev *et al.*, “Centrality determination of Pb-Pb collisions at $\sqrt{s_{\text{NN}}} = 2.76 \text{ TeV}$ with ALICE”, *Phys. Rev. C* **88** (2013) 044909, arXiv:1301.4361 [nucl-ex].
- [16] **ALICE** Collaboration, J. Adam *et al.*, “Centrality dependence of particle production in p-Pb collisions at $\sqrt{s_{\text{NN}}} = 5.02 \text{ TeV}$ ”, *Phys. Rev. C* **91** no. 6, (2015) 064905, arXiv:1412.6828 [nucl-ex].
- [17] **ALICE** Collaboration, S. Acharya *et al.*, “The ALICE definition of primary particles”, ALICE-PUBLIC-2017-005. <https://cds.cern.ch/record/2270008>.
- [18] **ALICE** Collaboration, J. Adam *et al.*, “Centrality evolution of the charged-particle pseudorapidity density over a broad pseudorapidity range in Pb-Pb collisions at $\sqrt{s_{\text{NN}}} = 2.76 \text{ TeV}$ ”, *Phys. Lett. B* **754** (2016) 373–385, arXiv:1509.07299 [nucl-ex].
- [19] **ALICE** Collaboration, J. Adam *et al.*, “Centrality dependence of the charged-particle multiplicity density at midrapidity in Pb-Pb collisions at $\sqrt{s_{\text{NN}}} = 5.02 \text{ TeV}$ ”, *Phys. Rev. Lett.* **116** (2016) 222302, arXiv:1512.06104 [nucl-ex].
- [20] **ALICE** Collaboration, S. Acharya *et al.*, “Charged-particle production as a function of multiplicity and transverse sphericity in pp collisions at $\sqrt{s} = 5.02$ and 13 TeV ”, *Eur. Phys. J. C* **79** no. 10, (2019) 857, arXiv:1905.07208 [nucl-ex].
- [21] S. J. Brodsky *et al.*, “Hadron Production in Nuclear Collisions: A New Parton Model Approach”, *Phys. Rev. Lett.* **39** (1977) 1120.
- [22] A. Adil *et al.*, “3D jet tomography of twisted strongly coupled quark gluon plasmas”, *Phys. Rev. C* **72** (2005) 034907, arXiv:nucl-th/0505004 [nucl-th].
- [23] **ALICE** Collaboration, E. Abbas *et al.*, “Centrality dependence of the pseudorapidity density distribution for charged particles in Pb-Pb collisions at $\sqrt{s_{\text{NN}}} = 2.76 \text{ TeV}$ ”, *Phys. Lett. B* **726** (2013) 610–622, arXiv:1304.0347 [nucl-ex].
- [24] **ALICE** Collaboration, S. Acharya *et al.*, “Centrality determination in heavy ion collisions”, ALICE-PUBLIC-2018-011. <http://cds.cern.ch/record/2636623>.

- [25] T. Pierog *et al.*, “EPOS LHC: Test of collective hadronization with data measured at the CERN Large Hadron Collider”, *Phys. Rev.* **C92** (2015) 034906, arXiv:1306.0121 [hep-ph].
- [26] ALICE Collaboration, B. Abelev *et al.*, “Centrality dependence of π , K, p production in Pb-Pb collisions at $\sqrt{s_{\text{NN}}} = 2.76 \text{ TeV}$ ”, *Phys. Rev.* **C88** (2013) 044910, arXiv:1303.0737 [hep-ex].
- [27] ALICE Collaboration, J. Adam *et al.*, “Measurement of transverse energy at midrapidity in Pb-Pb collisions at $\sqrt{s_{\text{NN}}} = 2.76 \text{ TeV}$ ”, *Phys. Rev.* **C94** no. 3, (2016) 034903, arXiv:1603.04775 [nucl-ex].
- [28] C. Loizides, J. Nagle, and P. Steinberg, “Improved version of the PHOBOS Glauber Monte Carlo”, *SoftwareX* **1-2** (2015) 13 – 18.
- [29] C. Loizides, “Glauber modeling of high-energy nuclear collisions at the subnucleon level”, *Phys. Rev. C* **94** no. 2, (2016) 024914, arXiv:1603.07375 [nucl-ex].